Radius of curvature of the *S* factor maximum in sub-barrier fusion hindrance

C. L. Jiang, B. B. Back, R. V. F. Janssens, and K. E. Rehm
Physics Division, Argonne National Laboratory, Argonne, Illinois 60439, USA
(Received 19 March 2007; published 30 May 2007)

A maximum of the $S(E)$ factor is evidence for an onset of sub-barrier fusion hindrance and it can be well described by a radius-of-curvature expression near the maximum. The systematics of this radius of curvature has been studied over a wide range of projectile-target combinations. It follows a tentative general trend as a function of the parameter $\zeta = Z_1 Z_2 \sqrt{\mu}$, and is strongly affected by effects associated with the nuclear structure of the nuclei in the entrance channel. It also explains the reason why the S factor maximum is not easily recognized visually for lighter, astrophysically interesting fusion systems.

DOI: 10.1103/PhysRevC.75.057604 PACS number(s): 25.60.Pj, 21.10.Pc, 25.70.Jj

It was recently been demonstrated that the appearance of sub-barrier fusion hindrance in heavy-ion fusion reactions is associated with a maximum in the astrophysical S factor [1]. Here, the S factor is given as $S = \sigma E e^{2\pi\eta}$, where η is the Sommerfeld parameter, $\eta = Z_1 Z_2 e^2/(\hbar v)$, v is the relative velocity of the two heavy ions and Z_1 and Z_2 are their respective atomic numbers, σ is the fusion cross section and E is the center of mass energy. The energy corresponding to the maximum is denoted E_s and the corresponding logarithmic derivative of the cross section is denoted L_s. Since

$$dS/dE = S(E)[L(E) - \pi\eta/E] \tag{1}$$

is zero at $E = E_s$, the logarithmic derivative for a function of constant S factor is [1]

$$L_{cs}(E) = \frac{\pi\eta}{E}, \quad \text{and} \quad L_s = L_{cs}(E_s). \tag{2}$$

Furthermore, the radius of curvature, ρ, of $\ln S$ at the maximum is given by

$$\frac{1}{\rho} = \left|\frac{d^2 \ln S}{dE^2}\right| = \left|\frac{dL}{dE} - \frac{d(\pi\eta/E)}{dE}\right| \quad \text{at} \quad E = E_s, \tag{3}$$

i.e., ρ is determined by the difference of derivatives from the logarithmic derivative of the experimental cross section, $L(E)$, and that corresponding to a constant S factor, $L_{cs}(E)$.

In this work we explore the systematics of the radius of curvature at the S factor maximum. Previously, we have found that E_s follows an overall systematics over a wide range of projectile-target combinations as a function of the parameter $Z_1 Z_2 \sqrt{\mu}$ [2–4], where μ is the reduced mass number. In addition, E_s appears to depend sensitively on the nuclear structure of the interacting nuclei. As demonstrated in Fig. 1, the logarithmic derivative, $L(E)$, near E_s is much steeper for the stiff system ^{58}Ni + ^{58}Ni, than for the open-shell system ^{64}Ni + ^{64}Ni [4]. Correspondingly, the S factor curve for ^{58}Ni + ^{58}Ni is much narrower than for ^{64}Ni + ^{64}Ni, see Fig. 1(b). The solid curves in Fig. 1(b) represent second-order Taylor expansions of $\ln S(E)$ around the S factor maximum such that

$$S = S_0 e^{-(E-E_s)^2/2\rho}, \tag{4}$$

where S_0 is the value of the S factor at its maximum.

Following the approach of Ref. [4], we have examined the radius of curvature of the S factor maximum for a number of systems for which the fusion cross sections have been studied down to small cross sections. The systems are divided into four categories depending on their "stiffness" and whether an S factor maximum was observed or an extrapolation was required to project the location of the maximum (see Table I). The radius of curvature is in all cases derived from the difference in logarithmic derivatives between the data and the constant S factor expression according to Eq. (3). Categories I and II refer to systems for which an S factor maximum has been observed in either "stiff" or "soft" systems, whereas extrapolation methods have been used to obtain the slopes of the logarithmic derivatives near E_s for category III systems. For light (category IV) systems, the slope was determined by fitting a function of the form $L(E) = A_0 + B_0/E^{3/2}$ to the data, see Refs. [4,27].

In order to understand the general trend of ρ, absolute values of the logarithmic derivatives $dL_{cs}(E)/dE$ and $dL(E)/dE$ at the energy E_s and the corresponding ratio of these two quantities,

$$RR = \frac{dL(E)/dE}{dL_{cs}(E)/dE}, \tag{5}$$

are shown in Figs. 2(a), 2(c), and 2(b) as a function of the parameter $\zeta = Z_1 Z_2 \sqrt{\mu}$, respectively. Aside from the local fluctuations, in general, $|L'_{cs}(E_s)|$ and RR are changing monotonically with ζ, i.e., the overall mass of the fusing system. The systematics of the energy E_s, the slope ratio RR and the logarithmic derivative L_s at E_s have been discussed in Ref. [4].

By using the definition of $dL_{cs}(E)/dE$ (Eq. (2)) and the emprical equation of L_s [4] (see[1]):

$$L_s = 2.33 + 500/\zeta \quad (\text{MeV}^{-2}), \tag{6}$$

the absolute value of $dL_{cs}(E)/dE$ at E_s can be obtained. This is shown by the solid curve in Fig. 2(a), which describes the experimental values quite well. In this paper, an empirical solid

[1]Because more data are included and some of the uncertainties have been reduced, the value of the parameter in Eq. (3) of Ref. [4] has been changed to 500.

TABLE I. This table lists the values of the quantities $\zeta = Z_1 Z_2 \sqrt{\mu}$, E_s, $(dL/dE)_{\rm exp}$, $(dL/dE)_{cs}$ and the radius-of-curvatures, ρ obtained from the two slopes at E_s. Q is the fusion Q-value. Systems in categories I and II exhibit a clear maximum in the $S(E)$ curve for "stiff" and "soft" systems, respectively. A maximum has not quite been reached for systems in category III; extrapolated values of E_s, $(dL/dE)_{\rm exp}$ and $(dL/dE)_{cs}$ are listed. For category IV, a least squares fit of $L(E) = A_0 + B_0/E^{3/2}$ is used to determine the values E_s and others. Uncertainties are included in parentheses. In general the Q-value is positive at small value of the parameter $Z_1 Z_2 \sqrt{\mu}$ and decreases (though not monotonically) to large negative values for large ζ. (In order to keep the table to a manageable size, some systems studied previously with the extrapolation method, have not been included. It was verified that the removal of these systems does not affect the fits and conclusions of the present work.)

System	$Z_1 Z_2 \sqrt{\mu}$	E_s (MeV)	$(dL/dE)_{\rm exp}$ (MeV^{-2})	$(dL/dE)_{cs}$ (MeV^{-2})	ρ (MeV^2)	Q (MeV)	Ref.
Category I							
^{90}Zr + ^{90}Zr	10733	175.2(1.8)	−1.61(0.16)	−0.020	0.63(0.06)	−157.35	[6]
^{90}Zr + ^{89}Y	10436	170.8(1.7)	−1.12(0.08)	−0.020	0.91(0.07)	−151.53	[6]
^{90}Zr + ^{92}Zr	10792	170.4(1.7)	−0.82(0.07)	−0.021	1.25(0.11)	−153.71	[6]
^{58}Ni + ^{58}Ni	4222	94.1(0.9)	−1.64(0.31)	−0.036	0.62(0.12)	−66.122	[5]
^{60}Ni + ^{89}Y	6537	122.6(1.2)	−0.49(0.07)	−0.029	2.16(0.34)	−90.497	[8]
^{32}S + ^{89}Y	3026	72.6(0.7)	−0.58(0.15)	−0.050	1.90(0.55)	−36.597	[9]
Category II							
^{64}Ni + ^{100}Mo	7343	120.6(1.2)	−0.58(0.09)	−0.034	1.84(0.31)	−92.287	[3]
^{64}Ni + ^{64}Ni	4435	87.5(0.9)	−0.35(0.03)	−0.046	3.26(0.34)	−48.783	[2]
^{28}Si + ^{64}Ni	1729	45.6(0.5)	−0.40(0.03)	−0.091	3.29(0.27)	−1.787	[7]
Category III							
^{90}Zr + ^{96}Zr	10899	165.3(4.9)	−0.37(0.05)	−0.023	2.8(0.4)	−62.03	[6]
^{58}Ni + ^{74}Ge	5106	97.4(2.9)	−0.56(0.18)	−0.041	1.9(0.7)	−62.03	[10]
^{64}Ni + ^{74}Ge	5249	96.4(2.9)	−0.49(0.08)	−0.043	2.2(0.4)	−58.48	[10]
^{58}Ni + ^{60}Ni	4258	92.0(1.8)	−0.67(0.07)	−0.039	1.59(0.17)	−62.69	[11]
^{58}Ni + ^{64}Ni	4325	89.4(1.8)	−0.79(0.30)	−0.043	1.3(0.5)	−53.04	[10]
^{36}S + ^{90}Zr	3244	74.1(1.1)	−0.72(0.13)	−0.051	1.49(0.29)	−36.76	[12]
^{36}S + ^{96}Zr	3273	72.1(1.1)	−0.87(0.05)	−0.055	1.23(0.07)	−27.67	[12]
^{28}Si + ^{58}Ni	1703	49.5(0.7)	−0.42(0.06)	−0.073	2.9(0.5)	−17.16	[13]
^{28}Si + ^{62}Ni	1721	48.5(0.7)	−0.74(0.29)	−0.078	1.5(0.7)	−8.07	[13]
^{30}Si + ^{58}Ni	1742	48.0(1.0)	−0.42(0.09)	−0.081	3.0(0.8)	−11.96	[13]
^{30}Si + ^{62}Ni	1762	45.9(0.9)	−0.31(0.08)	−0.091	4.6(1.7)	−4.37	[13]
^{30}Si + ^{64}Ni	1771	47.3(0.9)	−0.45(0.12)	−0.086	2.8(0.9)	−3.12	[13]
^{32}S + ^{58}Ni	2034	56.0(0.8)	−0.42(0.08)	−0.064	2.8(0.6)	−20.94	[13]
^{32}S + ^{64}Ni	2068	51.6(1.1)	−0.35(0.10)	−0.080	3.8(1.5)	−7.04	[13]
^{34}S + ^{58}Ni	2073	54.6(0.8)	−0.38(0.11)	−0.070	3.2(1.1)	−15.75	[13]
^{34}S + ^{64}Ni	2110	53.4(0.8)	−0.51(0.13)	−0.075	2.3(0.7)	−8.81	[13]
^{36}S + ^{58}Ni	2110	51.4(1.0)	−0.28(0.07)	−0.083	5.0(1.8)	−8.32	[13]
^{36}S + ^{64}Ni	2149	53.4(1.1)	−0.45(0.10)	−0.077	2.7(0.7)	−8.58	[13]
^{48}Ca + ^{48}Ca	1960	48.2(1.0)	−0.60(0.03)	−0.090	1.96(0.12)	−2.988	[14]
^{16}O + ^{76}Ge	930.5	27.6(0.8)	−0.35(0.03)	−0.172	5.5(1.0)	10.506	[15]
Category IV							
^{16}O + ^{16}O	181.0	6.79(0.27)	−2.04(0.20)	−1.12	1.09(0.27)	16.542	[16–20]
^{12}C + ^{16}O	125.7	4.39(0.18)	−3.04(0.10)	−2.30	1.35(0.42)	16.756	[16,21–23]
^{12}C + ^{14}N	106.8	3.49(0.14)	−4.27(0.45)	−3.49	1.3(1.0)	15.074	[16]
^{12}C + ^{13}C	89.9	3.45(0.17)	−4.02(0.15)	−3.02	1.0(0.4)	16.318	[16]
^{12}C + ^{12}C	88.2	3.68(0.15)	−3.05(0.07)	−2.51	1.9(0.9)	13.934	[24–26]
^{11}B + ^{12}C	71.9	2.12(0.13)	−9.4(0.3)	−8.12	0.8(0.7)	18.198	[16]
^{10}B + ^{10}B	55.9	1.47(0.10)	−18.(13.)	−15.9	0.5(0.4)	31.144	[16]

curve RR is given in Fig. 2(b) as (see[2])

$$RR = 1.10 + 1.70 \times 10^{-3}\zeta + 9.48 \times 10^{-8}\zeta^2. \quad (7)$$

[2]Because more data points are included, a new, better fit with a slightly different function as compared to Ref. [4] in Eq. (7) was chosen.

The absolute value of $L'(E_s)$ is then given by Eq. (5) and ρ can be obtained with Eqs. (2), (6), and (7) since

$$\rho = \frac{1}{(RR-1)|L'_{cs}(E_s)|}. \quad (8)$$

The dashed curves in Figs. 2(c) and 3(a) are calculated by Eqs. (5) and (8), respectively. They also

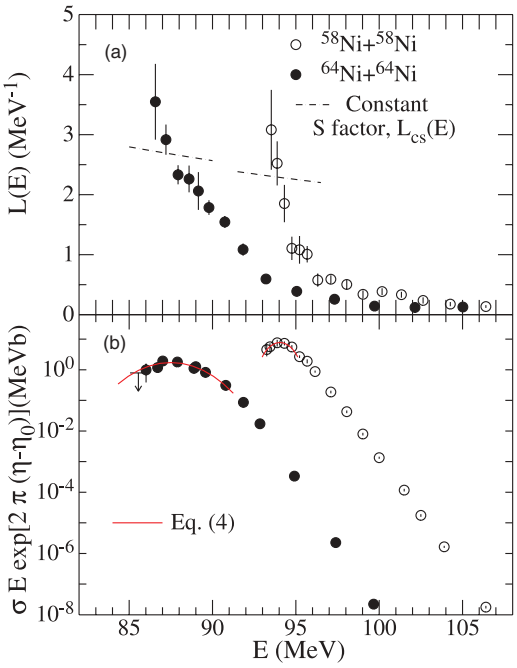

FIG. 1. (Color online) Logarithmic derivative representations (a) and S factor representations (b) for the systems ^{58}Ni + ^{58}Ni [5] and ^{64}Ni + ^{64}Ni [2], respectively. Solid curves are obtained with the description of the radius-of-curvature given by Eq. (4), see text for details. The adjustable parameter η_0 serves to put the two systems on a similar scale.

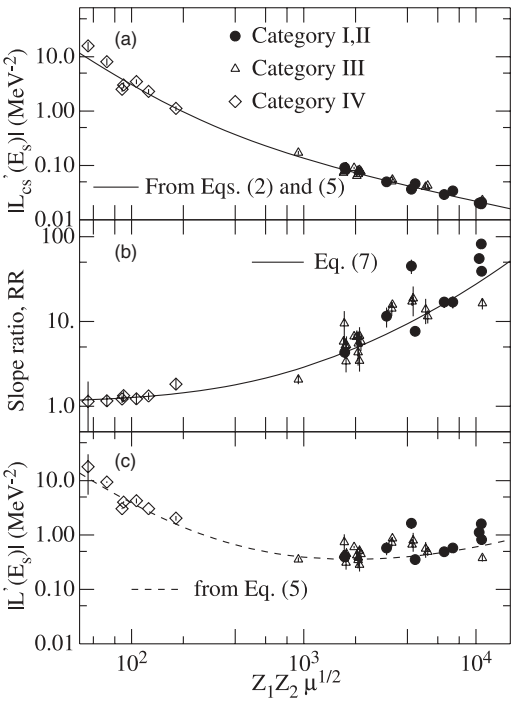

FIG. 2. Systematics of the absolute values of the logarithmic derivatives $dL_{cs}(E)/dE$ (a), the ratio $RR = \frac{dL(E)/dE}{dL_{cs}(E)/dE}$ (b) and the $dL(E)/dE$ (c) at energy E_s, respectively. The solid curves in (a) and (b) are empirical fitting functions. The dashed curve in (c) was obtained from the curves in (a) and (b).

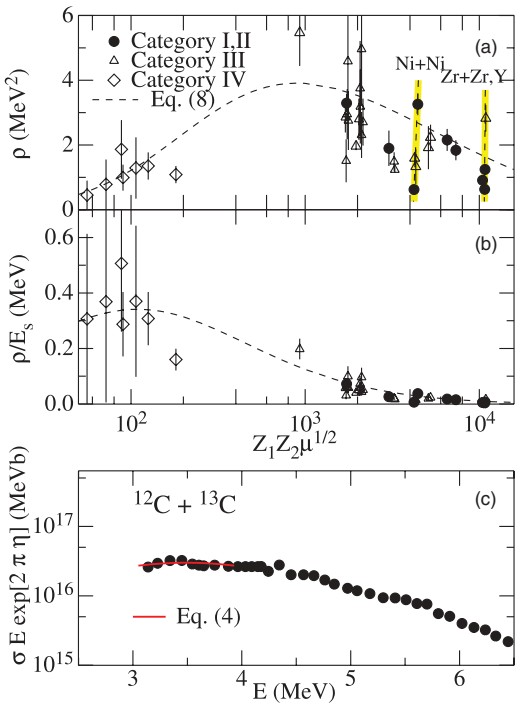

FIG. 3. (Color online) (a) Systematics of the radius-of-curvature of the S factor maximum. The absolute value of the radius-of-curvature, ρ, is plotted versus $Z_1 Z_2 \mu^{1/2}$. The vertical bands highlight the location of the Ni + Ni and Zr + Zr,Y systems. (b) Same as (a) but the ordinate has been divided by the value E_s. (c) $S(E)$ factor for the system ^{12}C + ^{13}C. The solid curve was obtained from Eq. (4). See text for details.

reproduce the general trends of these two functions rather well.

With the observed monotonic dependence of $|L'_{cs}(E_s)|$ and RR on the parameter ζ, the desired quantities, $|L'_{cs}(E_s)|$ and ρ show a minimum and a maximum as a function of ζ respectively, as illustrated in Figs. 2(c) and 3(a).

Thus a maximum of ρ appears at around $\zeta = 1000$, near the data point for the system ^{16}O + ^{76}Ge, i.e., in a region where the data were mostly obtained by extrapolation. It would, therefore, be of interest to perform more detailed experimental studies of some systems with the parameter ζ in the range, $\zeta \leqslant 1000$, to determine whether a maximum value of ρ occurs in this region.

In Fig. 3(b) we show the same data, but normalized to the energy E_s. Here, the dashed curve was obtained by using the systematics values of E_s, $E_s = (0.495\zeta/L_s)^{2/3}$ (Eqs. (2) and (6), see [4]). For the light fusion systems, from ^{10}B + ^{10}B to ^{16}O + ^{16}O, the value of ρ is rather large relative to its centroid value E_s. Futhermore the ratio ρ/E_s decreases by more than one order of magnitude, from about 0.35 to about 0.015 for heavier systems. If this ratio is large, the S factor maximum is not easily recognized visually. Thus, the determination of the sub-barrier hindrance effect in light systems represents a significant experimental challenge. A S factor representation is shown in Fig. 3(c) for the system ^{12}C + ^{13}C. The solid curve is obtained with the description of the radius of curvature given by Eq. (4). In this case it is difficult to recognize the S factor

maximum. This is an important result with consequences for studying the extrapolation of the S factors to very low energies for reactions of astrophysical interest [27].

Aside from the general trend discussed above and displayed in Fig. 3(a), large fluctuations of ρ around the average trend, represented by the dashed curve, are seen for systems of colliding nuclei of the same element, but with different masses. In particular, the systems highlighted by vertical bands, namely ^{58}Ni + ^{58}Ni, ^{58}Ni + ^{60}Ni, ^{58}Ni + ^{64}Ni, ^{64}Ni + ^{64}Ni and ^{90}Zr + ^{90}Zr, ^{90}Zr + ^{89}Y, ^{90}Zr + ^{92}Zr, ^{90}Zr + ^{96}Zr, show large deviations from the overall general trend. These systems range from "stiff" to "soft" colliding nuclei. These deviations emphasize a strong dependence of ρ on nuclear structure. To quantify this effect, the "softness" of a system has been expressed with a quantity, N_{ph}, defined as the proximity to closed proton or neutron shells with the number of "valence nucleons"; i.e., N_{ph} is the sum of particles and holes outside the nearest closed shells [3]. Plots of ρ versus N_{ph} are given in Fig. 4 for the systems Ni + Ni and Zr + Zr, Y. It is interesting to note that ρ is nearly proportional to the value of N_{ph} in each plot of Fig. 4 (dashed lines are the linear fits). Therefore, the radius of curvature of the S factor maximum appears to give another good measure of the "softness," i.e., of the impact of nuclear structure effects on the fusing systems.

Recently, the sub-barrier fusion hindrance (S factor maximum) has been reproduced well for the fusion reactions ^{64}Ni + ^{64}Ni and ^{28}Si + ^{64}Ni by a new calculation, which includes explicitly the saturation property of nuclear matter in the nuclear potential [7,28]. It would be very interesting to see whether this new theoretical approach could be developed further to study the systematics observed in the present paper and in Ref. [4].

In conclusion, the systematics of the radius of curvature of the S factor maximum has been studied in a number of systems where this behavior has been directly observed or inferred from an extrapolation of existing data. The radius of curvature is found to follow a tentative systematic trend as a function of the parameter $\zeta = Z_1 Z_2 \sqrt{\mu}$, representing the overall mass of the fusing system. However, as observed previously in the systematics of the fusion hindrance onset, the general trend can be strongly affected by effects associated with the structure of the nuclei involved [4]. It also exhibits the pattern that the S factor maximum is not easily recognized for lighter fusion systems of astrophysical interest [27].

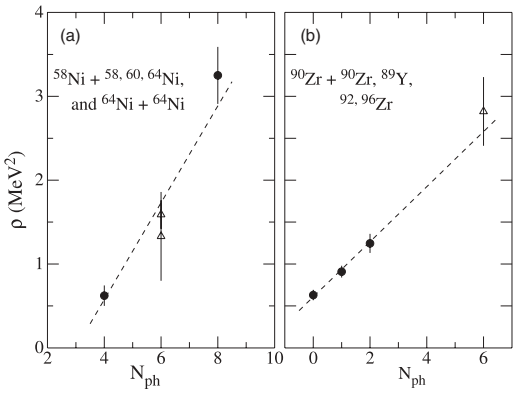

FIG. 4. Plots of ρ versus N_{ph} for reactions of Ni + Ni and of Zr + Zr, Y, respectively, where N_{ph} is the total number of "valence nucleons" outside closed shells in the entrance channel. Dashed lines are linear fittings.

The authors thank H. Esbensen for valuable discussions. This work was supported by the U.S. Department of Energy, Office of Nuclear Physics, under Contract No. DE-AC02–06CH11357.

[1] C. L. Jiang, H. Esbensen, B. B. Back, R. V. F. Janssens, and K. E. Rehm, Phys. Rev. C **69**, 014604 (2004).
[2] C. L. Jiang *et al.*, Phys. Rev. Lett. **93**, 012701 (2004).
[3] C. L. Jiang *et al.*, Phys. Rev. C **71**, 044613 (2005).
[4] C. L. Jiang, B. B. Back, H. Esbensen, R. V. F. Janssens, and K. E. Rehm, Phys. Rev. C **73**, 014613 (2006).
[5] M. Beckerman, T. Ball, H. Enge, M. Salomaa, A. Sperduto, S. Gazes, A. DiRienzo, and J. D. Molitoris, Phys. Rev. C **23**, 1581 (1981).
[6] J. G. Keller, K.-H. Schmidt, F. P. Hessberger, G. Munzenberg, and W. Reisdorf, Nucl. Phys. **A452**, 173 (1986).
[7] C. L. Jiang *et al.*, Phys. Lett. **B640**, 18 (2006).
[8] C. L. Jiang *et al.*, Phys. Rev. Lett. **89**, 052701 (2002).
[9] A. Mukherjee, M. Dasgupta, D. J. Hinde, K. Hagino, J. R. Leigh, J. C. Mein, C. R. Morton, J. O. Newton, and H. Timmers, Phys. Rev. C **66**, 034607 (2002).
[10] M. Beckerman, M. Salomaa, A. Sperduto, J. D. Molitoris, and A. DiRienzo, Phys. Rev. C **25**, 837 (1982).
[11] A. M. Stefanini *et al.*, Phys. Rev. Lett. **74**, 864 (1995).
[12] A. M. Stefanini, L. Corradi, A. M. Vinodkumar, Yang Feng, F. Scarlassara, G. Montagnoli, S. Beghini, and M. Bisogno, Phys. Rev. C **62**, 014601 (2000).
[13] A. M. Stefanini *et al.*, Nucl. Phys. **A456**, 509 (1986); Phys. Rev. C **30**, 2088 (1984).
[14] M. Trotta, A. M. Stefanini, L. Corradi, A. Gadea, F. Scarlassara, S. Beghini, and G. Montagnoli, Phys. Rev. C **65**, 011601(R) (2001).
[15] E. F. Aguilera, J. J. Kolata, and R. J. Tighe, Phys. Rev. C **52**, 3103 (1995).
[16] R. G. Stokstad *et al.*, Phys. Rev. Lett. **37**, 888 (1976).
[17] H. Spinka *et al.*, Nucl. Phys. **A233**, 456 (1974).
[18] S. C. Wu and C. A. Barnes, Nucl. Phys. **A422**, 373 (1984).
[19] J. Thomas, Y. T. Chen, S. Hinds, K. Langanke, D. Meredith, M. Olson, and C. A. Barnes, Phys. Rev. C **31**, 1980 (1985).
[20] G. Hulke *et al.*, Z. Phys. A **297**, 161 (1980).
[21] B. Čujec *et al.*, Nucl. Phys. **A266**, 461 (1976).
[22] Z. E. Switkowski *et al.*, Nucl. Phys. **A274**, 202 (1976).
[23] J. R. Patterson *et al.*, Nucl. Phys. **A165**, 545 (1971).
[24] L. J. Partterson, H. Winkler, and C. S. Zaidins, Astrophys. J. **157**, 367 (1969).
[25] M. Mazarakis and W. E. Stephens, Phys. Rev. C **7**, 1280 (1973).
[26] M. D. High and B. Čujec, Nucl. Phys. **A282**, 181 (1977).
[27] C. L. Jiang, K. E. Rehm, B. B. Back, and R. V. F. Janssens, Phys. Rev. C **75**, 015803 (2007).
[28] Ş. Mişicu and H. Esbensen, Phys. Rev. Lett. **96**, 112701 (2006).